Mica sheets with embedded metal nanorods: Chemical imaging in a topographically smooth structure

Malgorzata Graca and Jeff Turner
Department of Materials Science and Engineering, University of Illinois, Urbana, Illinois 61801; Department of Chemistry, University of Illinois, Urbana, Illinois 61801; and Department of Physics, University of Illinois, Urbana, Illinois 61801

Michael Marshall
Center for Microanalysis of Materials, Frederick Seitz Materials Research Laboratory, University of Illinois, Urbana, Illinois 61801

Steve Granick[a)]
Department of Materials Science and Engineering, University of Illinois, Urbana, Illinois 61801; Department of Chemistry, University of Illinois, Urbana, Illinois 61801; and Department of Physics, University of Illinois, Urbana, Illinois 61801

(Received 24 June 2007; accepted 19 July 2007; published online 21 September 2007)

We demonstrate the concept to combine topographical smoothness and plasmonic properties to produce flat substrates with surface enhanced Raman spectroscopy activity—properties that may find use in nanotribology and other thin film applications. Preliminary findings to this end are described. A dual-beam focused ion beam (FIB) system is used to drill large arrays of small pores in single crystals of mica, 2–6 μm thick, yielding controlled cross sections (squares, triangles, and circles), sizes (100 nm to many microns), and arrangements (square, hexagonal, and random). When filled with metals, arrays result to embedded nanorods with their long axis oriented normal to the surface. As an extension of this method, arrays of nanorods standing perpendicular to a supporting surface can also be produced. © *2007 American Institute of Physics*. [DOI: 10.1063/1.2777125]

During the past decade, applications utilizing metal nanowires and nanorods have burgeoned,[1–3] in large part because of expanding capabilities to fabricate these structures using a wide array of techniques. Originally used primarily to enhance electromagnetic fields for plasmonic devices, especially surface enhanced Raman spectroscopy (SERS),[4] metal nanostructures have recently found additional applications in areas as diverse as mechanical studies, sensing applications, and cancer screening and treatment. However, while many synthetic methods exist capable of producing structures of this kind, as a rule, they present a topographical perturbation to the environment.

This letter mainly concerns the use of plasmonic properties to study confined systems—systems confined in one or more directions to near-molecular spacings. When interrogating these buried sysems using surface enhanced vibrational spectroscopy, a limitation is that methods to enhance the Raman signal at the same time produces a topographically rough surface.[4] Here, we present preliminary findings directed toward the goal of enhancing the signal from vibrational spectroscopy while at the same time maintaining topographical smoothness to the extent possible.

UNMET NEEDS FOR NANOPATTERNING MICA

In studies of buried fluid interfaces, muscovite mica plays a central role because it is easily cleaved to produce large, step-free atomically smooth crystals. When these crystals are placed in close proximity, the surface-surface spacing can be quantified with angstrom accuracy. However, while force-based studies of systems based on this design are copious and have led to major advances,[5] a major limitation is the paucity of direct spectroscopic measurements of confined fluids. Earlier, this laboratory reported chemical imaging of fluids confined between muscovite micas using simple Raman spectroscopy—unenhanced by surface-specific effects[6]—but the signal to noise in those experiments, for fluids of nanometer thickness, was problematically low. The approaches described below present a first step to remedy this deficiency.

Muscovite mica is a mineral consisting of an aluminum-rich oxide layer sandwiched between silicon oxide layers. The sandwich structures are stacked further by a layer of potassium cations between the negative silicon oxide layers. This layered structure offers distinct advantages; with practice, mica can be cleaved along the basal plane, producing atomically smooth surfaces several cm^2 in area. The thickness of a single cleaved piece of mica can be controlled over a wide range as thin as ≈ 1 μm, simply by splitting manually. However, the layered structure also leads to limitations. The extended bonding in the lateral direction makes it extremely difficult to etch a nanopattern in the direction perpendicular to the cleavage plane. Standard lithography, optical and electron, is not usable on this surface, as one cannot etch grooves or pits. Other methods such as masking and etching (even in etchants as strong as NaOH, HF, or other strong acids) have no effect on the mica lattice.

To pattern mica surfaces, an approach reported by Müller *et al.*[7] consists of dragging the tip of a scanning probe

[a)]Electronic mail: sgranick@uiuc.edu

microscope across the surface, producing patterns of drawn lines, nanometer thick in the lateral dimension and depth, and as long as the microscope's piezoelectric positioning will allow. If one seeks to pattern the mica to create patterns wider than the sharp end of the tip or deep into the mica with a higher aspect ratio of depth to width, this method is not applicable.

The only successful approach in the literature to produce patterns that extend deeply into mica with nanometer lateral dimension is the so-called micromachining by ion track etching (MITE) method. This method is based on the experiments of Fleischer *et al.* in the early 1900s,[8] which bombarded mica samples with fission fragments from the neutron-induced fission of ^{235}U. The tracks produced in the mica by the heavy ions were visible as black lines in a TEM. Later work showed that these tracks were traces of slight atomic displacement (weakening) in the lattice structure, and that this weakened mica could be etched with HF. In subsequent experiments, different fission products (^{238}U and ^{232}Th) were employed, and the tracks were controlled to penetrate perpendicular to the mica surface.[9] Etching these holes produces nanopores, from tens of nanometer to microns in size, penetrating the entire thickness of mica up to 5 μm thick. This method is attractive, yet lacks control. As the nuclear ions bombard mica in a random pattern, patterned arrays cannot be produced. Also, the HF etch step is found (owing to the crystal structure of muscovite mica) to produce only diamond-shaped pores. Other shapes and controlled arrangements are impossible with this technique.

In the early 1970s, Possin reported the formation of nanowires in these pores via electroplating.[10] This technique has been advanced and applied to the formation of various metal wires and alloys, and interesting magnetic properties of these nanosystems have been measured.[11]

FORMATION OF PATTERNED ARRAYS EMBEDDED WITHIN MICA

The methods described below employ a dual-beam focused ion beam (FIB) instrument (FEI Company model 235), as sketched in Fig. 1(a). First, a mica sheet is cleaved in a laminar flow cabinet to a thickness controlled between 2 and 6 μm. Next, for geometrical support, this mica sheet is placed onto a freshly cleaved thicker sheet of mica (backing sheet). The exposed side of the thin sheet is coated with 20 nm of gold to act as a conductive layer for beam focusing, and this substrate is subsequently introduced into the chamber of the FIB. The computer-programed pattern to be drilled through the thin mica is produced either as a bitmap image or a script program, and etching proceeds at high current (500–7000 pA) with a focused beam of 30 kV Ga^+ ions. The cross section of the pattern can be circular, square, triangular, diamond shaped, or any other shape drawn in the bitmap. The minimum spot size of the ion beam is 7 nm. Etching entirely through a 5 μm thick sheet can be accomplished with circular pores as small as 30 nm diameter, and sharp edges are obtainable in square and triangular pores with cross-sectional size as small as 200 nm. Depending on the exact current used and the pore size and mica thickness, a single pore is drilled in 2–20 s, typically. The pores are oriented perpendicular to the surface of the mica, and the walls are fairly vertical, as evidenced by the nanorods described and characterized below. Pore arrays as large as 500×500 have been produced in our laboratory; the theoretical limits to the array size are only the size of the FIB stage, currently a 2.5 cm circle and the time to drill the desired number of holes.

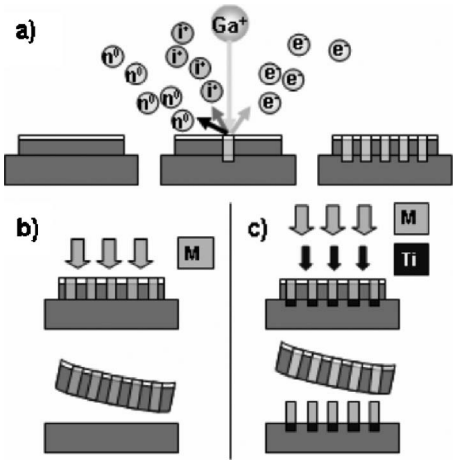

FIG. 1. Schematic representation of the nanofabrication process. (a) A freshly cleaved mica sheet is placed on a thicker backing sheet and coated with 20 nm of Au. Using a dual-beam focused ion beam, Ga^+ ions focused to the surface are used to etch a programed array of nanopores. The pores extend through the mica and ≈50 nm into the backing sheet. (b) The thin mica sheet is removed and placed on a second freshly cleaved backing sheet. Electron-beam sputtering is used to implant a metal (M) into the pores. Next, the thin mica sheet is mechanically peeled form the backing sheet, producing a mica sheet with embedded nanorods. (c) Alternatively, free-standing nanorods are produced using a variant of this process. After process (a), the perforated mica sheet is placed in an electron-beam chamber. A 10–20 nm adhesion layer of Cr or Ti is deposited, metal is deposited on top of that, and finally the thin mica sheet is removed mechanically, leaving an array of nanorods oriented perpendicular to the backing sheet.

Figure 2 illustrates scanning electron micrograph (SEM) images obtained using the e-beam capabilities of the dual-beam instrument. Figure 2(a) shows a square array of square

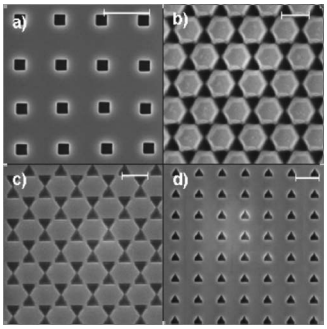

FIG. 2. Illustrations of various cross sections, spacings, and arrangements of pores produced using the methods summarized in Fig. 1. These are images collected via SEM in the dual-beam FIB. (a) A square array of square cross section pores of width of 300 nm, deposited in a mica sheet 3 μm thick. (b) A hexagonal array of triangular cross section pores of width of 500 nm, deposited in a mica sheet 6 μm thick. Notice the distortions at the edges, discussed in the text. (c) Triangles with the same parameters as in panel (b), except etched through a mica sheet 4 μm thick. Notice the higher quality edges. (d) A square array of triangular cross section pores of width of 400 nm etched through a mica sheet 3 μm thick. The scale bar is 1 μm.

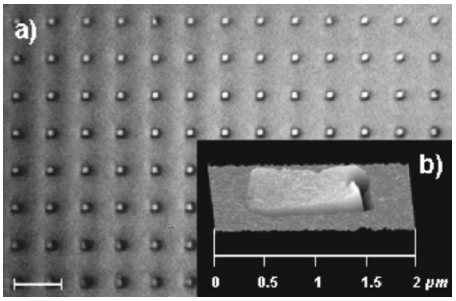

FIG. 3. Illustration of quality in these patterns. (a) An optical micrograph of a small section of a 500×500 array of embedded rods with square cross section, 1 μm wide, and 3 μm long, produced using the method in Fig. 1(b). Defect density in the array is approximately 1%. (b) An AFM image of the top surface of one of these rods, showing the smoothness of the surface. In this typical image, the rod protrudes 4.5 nm from the mica and a small valley near the edge is inset by 3 nm. Overall, the RMS roughness of a 50×50 μm^2 portion of the array was measured by AFM to be 1.5 nm. The scale bar is 1 μm.

cross section pores of width of 300 nm, etched through a sheet of mica 3 μm in thickness. Figure 2(b) shows a hexagonal array of triangles in mica 6 μm thick. It should be noticed in Fig. 2(b) that the edges of the triangles are blurred. Drilling through a sheet of this large thickness becomes problematic since the angle of the focused beam causes some rounding on the top edge when milling near the bottom of the sample. The high current used in these experiments can increase this effect. When the identical pattern is produced in a mica sheet 4 μm thick, the sharper pattern in Fig. 2(c) is obtained. Figure 2(d), showing triangles arranged in a square pattern, illustrates the diverse patterns that can be obtained.

To create nanorods, the procedure shown schematically in Fig. 1(b) is employed. First, the thin porous mica is mechanically peeled from its backing sheet and placed clean side down on a fresh backing sheet. Next, the pores are filled using an e-beam sputtering system (Temescal, BOC Edwards, Inc.). In principle, any material compatible with the e-beam can be deposited, including semiconductors, insulators such as the oxides of titanium, aluminum, or silicon, and numerous metals.

In our experiments, gold, silver, aluminum, and copper have been used. The metals are deposited at 10^{-7} torr with an e-beam power producing a deposition rate of 0.1–0.3 nm/s. The aspect ratio of the nanorod is controlled by setting the width of the pore and subsequently controlling the thickness of metal introduced into the pore. Due to technical limitations of the process, presently, the maximum aspect ratio is limited to ~15. After metal deposition, the mica sheet containing the embedded nanorod array is removed from the backing sheet. Since the metals used in this experiment have low adhesion to mica, the nanorods do not stick to the backing sheet and remain within the pores.

Figure 3 shows an array of square embedded gold rods, produced with a large cross section (1 μm) in order to enable imaging of the 500×500 array using an optical microscope. The long axis of the rods is 3 μm in length, and the mica that envelops them is 5 μm thick. Figure 3(a) shows a small 13×8 rod slice of this array, and it should be noticed that no defects are evident. In the case of these embedded rods, a defect density of less than 1% was observed.

The inset [Fig. 3(b)], shows an atomic force micrograph (Dimension 3100, Veeco) of the mica surface and one of these embedded rods. The rod protrudes 4.5 nm from the surface and a small valley near the edge is inset by 3 nm. The valley is formed due to the poor wetting of mica by gold, and we attribute the peak to the buildup of material missing from the valley coupled to damage during the mechanical removal from the backing sheet. The root mean square (RMS) roughness of a 50×50 μm^2 atomic force micrograph (AFM) (MFP-3D, Asylum Research) of this sample surface is 1.5 nm. This substrate is close to being topographically flat, yet "rough" in terms of dielectric coefficient since gold is more optically dense than the enveloping mica.

A rational concern about this method might be that just the top of the pores would fill, leaving the bottoms empty. The freestanding rods visualized after removing the mechanical mask, described in the following section, demonstrate that this did not occur.

FORMATION OF FREESTANDING RODS

A slight modification to the fabrication scheme, sketched in Fig. 1(c), allows one to form arrays of freestanding nanorods with their long axis perpendicular to a supporting mica substrate. This scheme is predicated on using directly, without removal from the original backing sheet, the nanoporous thin mica single crystal produced via the process sketched in Fig. 1(a).

The pores are drilled to fully penetrate the thin mica sheet and penetrate slightly beyond it into the backing sheet. For example, if the mica sheet is 5 μm thick, the pores are drilled to a depth of 5.05 μm. The entire mica (backing sheet and thin porous mask) is then inserted into the e-beam sputtering system. A thin (10–20 nm) adhesion layer of Ti or Cr is coated onto the entire piece, thus depositing a thin Ti or Cr layer at the bottom of the pore. The metal (Au or Ag) is then deposited to the desired length of the eventual nanorod. In the final fabrication step, the thin mica mask is removed by mechanical lifting, being careful to keep the force in the direction normal to the surfaces. The adhesion layer anchors the nanorod to the backing sheet, which now acts as a support for the vertically aligned nanorods.

The solid mica mask is discarded or can be reused as a mask to create more nanorods on another substrate, provided it remains clean and intact. In some experiments, we have replaced the mica backing sheet with a clean Si wafer, and no differences were observed in quality of the product.

Figure 4 illustrates an array of square cross section (350 nm) nanorods in a square arrangement with lattice spacing of 1.1 μm and 1.0 μm rod height. The entire array was 50 rods$\times$50 rods, with a 7 rod$\times$5 rod subsection shown in this AFM (Dimension 3100, Veeco) for clarity. It should be noted that two of the rods near the center look as if they are stretched vertically to the surface. In this process, much care must be taken during the mechanical mask removal to avoid the deformation of the nanorods since fairly soft metals are used. Defects become more prominent, the

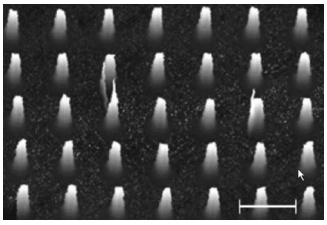

FIG. 4. Illustration of freestanding nanorods produced using the method in Fig. 1(c). This AFM image shows 350 nm square cross section rods 1 μm high with their long axis oriented perpendicular to the supporting mica surface. Taken from the fabricated 50×50 array of these rods, this image shows a subsection. The scale bar is 1 μm.

higher the height-to-width ratio. Defect densities are found to exceed 20% when the height-to-width ratio exceeds 5.

Structures with sharper corners are more difficult to produce with high aspect ratio. While square and circular nanorods can be produced with cross section down to 200 nm and aspect ratio as high as 5, triangular structures have only been successful with widths on the order of 350 nm and aspect ratio closer to 3. The long edges of smaller triangular structures tend to bend or break, losing sharpness.

DEMONSTRATING THE UTILITY OF THE STRUCTURES

The embedded metal structures shown in Fig. 3 find application in the enhancement of the Raman signal from a thin film of polymer coated on the mica surface. The Raman setup used in this experiment was homebuilt, consisting of a 488 nm Ar^+ introduced into a confocal microscope, where the incident laser is focused by and the signal collected by the same objective lens. Raman and Rayleigh scatterings are separated by a notch filter, and the Raman signal is routed to a 500 cm spectrometer with a liquid nitrogen–cooled charge-coupled device (CCD) camera by an optical fiber.

The substrate from Fig. 3 was spin coated with a 20-nm-thick film of polystyrene (PS). When the laser was focused on the film in an area more than 1 mm away from the embedded metal structures, the Raman spectrum shown as a red trace in Fig. 5 was collected. Because of the low thickness of the film, an acquisition time of 2 mins was required to collect a spectrum of this quality.

The embedded gold rods in this substrate were produced with a very large cross section to enable the imaging of the individual rods with an optical microscope. As such, we would expect a fairly low electric field enhancement at their surface since optimal nanostructures for SERS are of much smaller scale.[4] However, even on these nonoptimized embedded structures, enhancement is observed in the Raman signal from the PS film. When the laser spot is moved to the top of one of these structures, as confirmed through the viewfinder of the microscope, the SERS spectrum (black trace in Fig. 5) is collected. To collect a spectrum of this quality, an acquisition time of 15 s is required, as the field enhancement from the supporting metal structure strengthens the signal significantly. The enhancement factor for this spectrum, taking into account the thin-film Raman intensities and the acquisition times, depends on which PS vibration peak is considered but is in the range of $40\times-160\times$. The enhancement

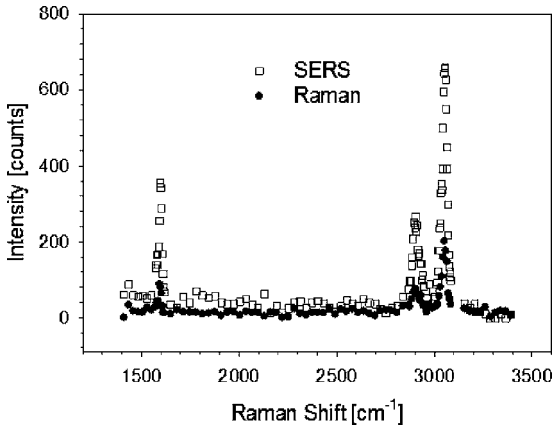

FIG. 5. Unenhanced Raman (filled symbols) and SERS (open symbols) spectra of a 20 nm polystyrene (PS) film on a mica substrate with embedded gold rods (Fig. 3). After spin coating the PS film on the mica, the laser spot was scanned from an area on neat mica away from the embedded rods, where the unenhanced Raman spectrum was collected (2 min acquisition time), to the tip of one of the embedded gold rods, where the SERS spectrum was collected (15 s acquisition time).

is not yet as large as has been produced using topographically rough SERS structures—the main point is the concept.

OUTLOOK

The methods discussed here allow one to produce nanorods composed of any metal easily deposited by electron beam. These patterned arrays are controllable in their aspect ratio, cross-sectional geometry, and arrangement on a surface. This method can also be used to form nanorods embedded within a substrate and oriented normal to it, thus producing a surface that is nearly flat topographically, yet chemically rough.

The main difference of this study was to employ muscovite mica, which is a translucent, flexible, dielectric substrate, easily cleaved to form single crystals that are atomically smooth over areas as large as cm^2. Since these mica substrates are thin, they offer the advantages of a geometrically flexible support. Most important, mica is clear from the visible through the near IR, and is electrically insulating. In these respects it offers distinct advantages over the silicon wafer substrates often utilized in nanofabrication schemes.

The embedded rod structures described here are envisioned to find their applications using SERS, as demonstrated in the proof-of-concept experiment detailed in Fig. 5, although it is expected that the quality of SERS measurements with these arrays can be improved. For plasmonic applications, structures smaller in size and with smaller distance between adjacent embedded metal rods will be useful,[12] but the path in that direction is clear, following up on the present proof-of-concept study. The difference in dielectric coefficients between the mica and the embedded metal, coupled with the sharp edges of our structures, also contributes to the promise for this application. A flat SERS substrate would offer considerable advantages over a conventional substrate, especially in biological, thin film, and nanotribology (surface forces) experiments. This technique may also find application in studies of polymer adsorption and desorption.[13,14]

ACKNOWLEDGMENTS

We thank Richard Van Duyne for a remark that inspired this work. One of us (J.T.) is grateful to Colgate-Palmolive for a Bioengineering Graduate Fellowship. One of us (M.G.) thanks the Foundation for Polish Science for a postdoctoral fellowship. This work was supported by the National Science Foundation, No. NSF-CMS-05-55820.

[1]H. He and N. J. Tao, *Encyclopedia of Nanoscience and Nanotechnology: Electrochemical Fabrication of Metal Nanowires*, edited by H. S. Nalwa (American Scientific Publishers, Stevenson Ranch, CA, 2003), Vol. 10.
[2]B. Wiley, J. Sun, B. Mayers, and Y. Xia, Chem.-Eur. J. **11**, 454 (2004).
[3]L. Sun, Y. Hao, C. L. Chien, and P. C. Searson, IBM J. Res. Dev. **49**, 79 (2005).
[4]W. H. Yang, G. C. Schatz, and R. P. Van Duyne, J. Chem. Phys. **103**, 869 (1995).
[5]J. N. Israelachvili, Intermolecular and Surface Forces (Wiley, New York, 1992).
[6]S. C. Bae, H. Lee, Z. Lin, and S. Granick, Langmuir **13**, 5685 (2005).
[7]M. Müller, T. Fiedler, R. Gröger, T. Koch, S. Walheim, Ch. Obermair, and T. Schimmel, Surf. Interface Anal. **36**, 189 (2004).
[8]R. L. Fleischer, P. B. Price, R. M. Walker, and E. L. Hubbard, Phys. Rev. **133**, A1443 (1964).
[9]M. Lang, U. A. Glasmacher, B. Moine, B. Neumann, and G. A. Wagner, Nucl. Instrum. Methods Phys. Res. B **218**, 466 (2004), and references therein.
[10]G. E. Possin, Physica (Utrecht) **55**, 339 (1971).
[11]L. Sun, P. C. Searson, and C. L. Chien, Phys. Rev. B **61**, R6463 (2000), and references therein.
[12]H. H. Wang *et al.*, Adv. Mater. (Weinheim, Ger.) **18**, 491 (2006).
[13]H. E. Johnson, J. F. Douglas, and S. Granick, Phys. Rev. Lett. **70**, 3267 (1993).
[14]H. M. Schneider, P. Frantz, and S. Granick, Langmuir **12**, 994 (1996).